Engineering cancer microenvironments for in vitro 3-D tumor models

Published in final edited form as:

Mater Today (Kidlington). 2015 December ; 18(10): 539–553. doi:10.1016/j.mattod.2015.05.002.

Engineering cancer microenvironments for *in vitro* 3-D tumor models

Waseem Asghar[1,2,5,*], **Rami El Assal**[1,5], **Hadi Shafiee**[3], **Sharon Pitteri**[4], **Ramasamy Paulmurugan**[4], and **Utkan Demirci**[1,3,4,*]

[1]Demirci Bio-Acoustic-MEMS in Medicine (BAMM) Laboratories, Department of Radiology, Canary Center at Stanford for Cancer Early Detection, Stanford School of Medicine, Stanford University, Palo Alto, CA 94304, USA

[2]Department of Computer Engineering & Electrical Engineering and Computer Science, Florida Atlantic University, Boca Raton, FL 33431, USA

[3]Demirci Bio-Acoustic-MEMS in Medicine (BAMM) Laboratories, Division of Biomedical Engineering, Division of Infectious Diseases, Renal Division, Department of Medicine, Brigham and Women's Hospital, Harvard Medical School, Cambridge, MA 02139, USA

[4]Department of Radiology, Canary Center at Stanford for Cancer Early Detection, Stanford School of Medicine, Stanford University, Palo Alto, CA 94304, USA

Abstract

The natural microenvironment of tumors is composed of extracellular matrix (ECM), blood vasculature, and supporting stromal cells. The physical characteristics of ECM as well as the cellular components play a vital role in controlling cancer cell proliferation, apoptosis, metabolism, and differentiation. To mimic the tumor microenvironment outside the human body for drug testing, two-dimensional (2-D) and murine tumor models are routinely used. Although these conventional approaches are employed in preclinical studies, they still present challenges. For example, murine tumor models are expensive and difficult to adopt for routine drug screening. On the other hand, 2-D *in vitro* models are simple to perform, but they do not recapitulate natural tumor microenvironment, because they do not capture important three-dimensional (3-D) cell–cell, cell–matrix signaling pathways, and multi-cellular heterogeneous components of the tumor microenvironment such as stromal and immune cells. The three-dimensional (3-D) *in vitro* tumor models aim to closely mimic cancer microenvironments and have emerged as an alternative to routinely used methods for drug screening. Herein, we review recent advances in 3-D tumor model generation and highlight directions for future applications in drug testing.

[*]Corresponding authors: Asghar, W. (wasghar@fau.edu), Demirci, U. (utkan@stanford.edu).
[5]These authors contributed equally to this study.

Conflict of interest statement

Dr. Utkan Demirci is a founder of, and has an equity interest in: (i) DxNow Inc., a company that is developing microfluidic and imaging technologies for point-of-care diagnostic solutions, and (ii) Koek Biotech, a company that is developing microfluidic IVF technologies for clinical solutions. Dr. Utkan Demirci's interests were viewed and managed in accordance with their conflict of interest policies.

Introduction

Tumor growth and aggressiveness are influenced by the microenvironment surrounding the tumor mass [1–5]. The native tumor microenvironment is composed of extracellular matrix (ECM), cell–cell contact, and cell–matrix interactions [6–8]. The ECM consists of a nanofibrous mesh of proteins (i.e., elastin, collagen, fibronectin, and laminin), which fill the extracellular spaces around the cells to help them stay connected with each other by adhesion proteins [9]. In addition, the ECM components are involved in various cell signaling pathways [10,11]. These cell–cell and cell–matrix interactions regulate tumor growth, angiogenesis, aggression, invasion, and metastasis (Fig. 1) [12,13]. In the early stages of cancer, tumor cells undergo certain alterations (a process called immunoediting) to initiate signaling pathways that inactivate the immune system to prevent their elimination from the body [14,15]. Such alterations allow cancer cells to avoid the body's immune response and grow abnormally to form a large tumor mass.

During immunotherapy, the native immune system is reactivated by administration of peripheral blood lymphocytes or immune modulatory drugs [16]. Various immunotherapy drugs have been introduced in the past to treat cancer patients, but many of them have not exhibited a good response during phase I/II clinical trials [17]. For example, the first immunotherapy (Sipuleucel-T, Provenge) for castration-resistant prostate cancer patients approved by United States Food and Drug Administration (FDA) prolonged the survival of cancer patients by only a couple of months as compared to standard drugs and placebo controls [18]. Furthermore, in many clinical trials, drug testing is also hampered by the limited enrollment of cancer patients [19]. Such drawbacks limit the development of new drugs for cancer patients.

Two-dimensional (2-D) *in vitro* cancer models and small *in vivo* animal models are used conventionally for drug testing and screening [20,21]. However, because of the difficulty in recapitulating the natural tumor microenvironment in 2-D culture as well as the cost and issues associated with animal models, both approaches have become less attractive for routine drug testing. New three-dimensional (3-D) *in vitro* cancer models have emerged as an alternative approach to conventional methods and have shown the potential to recapitulate the natural microenvironment of tumors in a relatively simple and inexpensive way when compared to conventional methods [22–29]. In this article, we review the significance and limitations of different tumor models used in the literature for drug testing. We also discuss various approaches that are currently available for generating 3-D tumor models such as spheroids, hanging drop, bio-printing, and magnetic levitation. In addition, we evaluate the effect of materials (e.g., basement membrane matrix, hydrogels, and scaffolds) and physical parameters (e.g., stiffness, morphology, flow, and shear stress) on the growth, invasiveness, differentiation, and regulation of biomarker expression of cancer cells. Finally, we highlight future directions for 3-D cancer models toward applications in anti-cancer drug development.

Strengths and limitations of 2-D *vs.* 3-D tumor models

Cancer cells are routinely cultured on 2-D plastic substrata in the pharmaceutical industry [30]. In 2-D tumor models, cancer cells are grown as a monolayer and do not mimic the native tumor environment [21,31]. The cells sit on a flat 2-D surface with almost half of the cell's surface directly bound to plastic substrata. Cancer cells grown on a 2-D surface lose certain signaling pathways that are important in defining cell's natural response in terms of growth, metabolism, and differentiation [31–34]. In one study, human breast tumor cell line (T4-2) derived from phenotypically normal cells (HMT-3522) cultured on 3-D basement model underwent concomitant down-regulation of epidermal growth factor receptor (EGFR) and β1-integrin when the cells were treated with antibody mediated inhibition factors [35]. The modulation of these receptors in 3-D tumor model led to growth arrest and finally reversion of malignant behavior of T4-2 cancer cells to normal breast tissue morphogenesis [35]. On the other hand, when T4-2 cancer cells were cultured on 2-D substrata and treated with antibody inhibition factors, no down-regulation and growth arrest were noticed [35]. In another report, a human breast cancer cell line (MCF-7) and its multidrug resistance variant (MDR-MCF-7) cells were cultured using 3-D spheroid and 2-D monolayer methods [36]. Both types of cancer cells showed reduced proliferation in 3-D culture as compared to 2-D monolayer culture. The cultured cancer cells were also treated with the anti-cancer drug doxorubicin. It was reported that MCF-7 cancer cells grown in the 3-D model had reduced sensitivity to doxorubicin as compared to 2-D cultures [36]. The MDR-MCF-7 cancer cells showed no response to drug treatment when cultured in a 3-D model. The invasive potential of MDR-MCF-7 cells was also increased when cultured in a 3-D model. Further, in the case of solid tumor, cancer cells are hypoxic at the center because of limited blood and oxygen supply [37,38]. This phenomenon cannot be mimicked in a 2-D culture model as cells grow in a single layer and every cell has continuous supply of oxygen and nutrients. These findings clearly pointed out that ECM composition and cell–matrix interactions play a vital role in cancer cell growth, metabolism, and invasiveness, and the complexity of the tumor microenvironment cannot be recapitulated in 2-D cancer cell culture models. Limitations of 2-D tumor models were also highlighted by other reviews in the field [39–41].

Strengths and limitations of animal models of human tumors (xenografts)

Xenograft animal models of human tumors are widely used as *in vivo* tumor models for studying cancer metastasis and drug screening [42,43]. In this model, cancer cells are subcutaneously injected into immunocompromised mice and allowed to grow for a couple of weeks. It has been reported that small cancerous tissues implanted in respective organs (orthotopic) of mice were used to study the invasive and metastatic properties of cancer cells [42]. The cancer cells grow, because the immunocompromised mice do not generate sufficient immune response to the xenograft of human cells. On the other hand, the xenograft model does not fully mimic the natural response of the human body [44], as the immunocompromised mice lack some growth factors such as interleukin-8 (IL-8) that are secreted in humans by immune cells. In the case of ovarian cancer, the mouse omentum is located close to the pancreas having different histological appearance as compared to human omentum [45]. These findings may partially explain why only 27% of drugs with good efficiency in animal models show no sensitivity during phase II clinical trials [46,47]. This

clearly indicates that alternative 3-D tumor models are required to better mimic the body's natural response and to allow direct observation of the tumor during the course of the treatment.

Technologies to develop 3-D cultures and spheroids

Tumor cells growing in conventional monolayer 2-D *in vitro* systems have limited ability to mimic the *in vivo* cell–cell and cell–matrix interactions [48,49]. However, when tumor cells are cultured in a 3-D *in vitro* system, they support each other and behave in a way that is similar to the *in vivo* system (e.g., adhesion, motility, invasiveness and metastasis) [50–53]. In addition, in 3-D culture endothelial and stromal cells can be mixed in a particular proportion allowing them to mimic cellular organization in human tumors, and exchange growth factors and other extracellular matrix proteins [54,55]. In the following sections, we discuss various tools currently available to develop 3-D cancer models along with material prospects. The strengths and limitations of each method are highlighted in the respective paragraphs.

Spheroids and hanging drops

Spheroid aggregation of cells is one of the easiest ways to culture tumor cells in 3-D [56]. Because of self-assembly, reproducibility, and similarity to native tissues, spheroid formation for 3-D tumor culture has become a well-characterized model [56–59]. Production efficiency, spheroid size uniformity, influence of cellular physiology, and suitability for subsequent application are the general criteria for selecting the spheroid production method [60]. Because of its simplicity, the hanging drop technique emerged among various other techniques (e.g., liquid-overlay and gyratory rotation methods) to promote 3-D spheroid formation through natural aggregation [61]. The gravity in the pipetted droplets concentrates cells at the liquid-air interface to generate spheroids when the lid is inverted. Although this method is simple and inexpensive to generate spheroids, high throughput and control of droplet size and uniformity are present challenges. Recently, microfluidic chips have been described to overcome the limitations of the conventional techniques; however, these spheroid-on-chips suffer from the difficulty of providing long-term cultures [62–66]. Additionally, the liquid handling robots, which perform high throughput screening are incompatible with the microfluidic approach [57]. A high-throughput 384 well hanging drop array was developed for spheroid formation, culture, and drug screening that is compatible with the existing liquid handing robots (Fig. 2a) [57,67]. By utilizing this approach, the researchers showed that the 3-D culture models of human epithelial carcinoma cells were more resistant (75% viability after 96 h) to anticancer drug 5-fluorouracil than cells evaluated in 2-D culture (5% viability after 96 h). However, 3-D cultured cells were less resistant (40%, compared with 75% in 2-D) to the hypoxia activated tirapazamine drug, where the active oxygen consumption and limited oxygen diffusion created a hypoxic and necrotic core, which synergized with the effect of the drug [57].

Despite its simplicity, the hanging drop technique based on manual pipetting is time-consuming and labor-intensive. The results vary between operators because of their technique and skill level. These technical limitations are also responsible for increased

mechanical stress on the cells, which affect the 3-D geometry of the droplet and 3-D structure of the culture system [68]. Furthermore, the non-homogeneous spreading of the droplet during manual pipetting leads to non-uniform cell densities in the droplet. In an attempt to overcome these challenges, a reproducible, efficient, and scalable method was developed to generate a more controllable uniform-sized 3-D culture by integrating the existing hanging-drop method with bio-printing technology (Fig. 2b) [68]. This combined approach is simple, robust, and reproducible, utilizing a valve-based bio-printing methodology that can generate 160 droplets per second. Generating an equal number of droplets (160 droplets) by the conventional manual pipetting method would take up to 10 min [68].

3-D bio-printing of cancer cells

In recent years, there has been increasing interest in integrating bio-printing technologies with stem cells, cell bio-preservation, and cancer research [69–81]. Cell printing is an emerging approach for 3-D cancer cell patterning, which provides control over spatial and temporal distribution of cell seeding [81–84]. In a recent study, a high-throughput automated bio-printing approach was utilized to pattern a 3-D co-culture model of human ovarian cancer cells and fibroblasts-encapsulated droplets with high cell viability (Fig. 3a) [70]. This approach provided reproducible control over spatial distance between cell types (i.e., cancer and stromal cells). Although other bio-printing methods (e.g., inkjet and laser printing) have been developed to control cell seeding in 2-D and 3-D models, these methods have some limitations (Fig. 3b and c) [78,85,86]. For successful delivery of bio-fluids, inkjet and laser technologies require certain design parameters to avoid damaging of pressure- and heat-sensitive fluids [69,87]. This is crucial when printing live cells, as they do not tolerate high temperature and stress [69,88,89]. Although inkjet printers are simple in design and can print various types of materials, it is difficult to achieve the directionality with the traditional inkjet devices as the ejection directionality is limited by the geometry of the nozzle [69]. As an alternative, an acoustic picoliter droplet ejector was designed for precise cell encapsulation in bio-fluids with high viability, and high directionality *via* an open-pool nozzleless ejection system actuated by an acoustic field [90,91]. The acoustic ejector is simple and performs reliably without generating excessive heat and pressure-sensitive fluids [69,90,91]. In summary, the bio-printing technology is an attractive approach for various applications in 3-D tumor models generation, tissue engineering, and regenerative medicine.

Cell assembly with and without magnetic nanoparticles

Utilization of non-invasive approaches such as magnetic levitation to assemble 3-D complex structures has recently been demonstrated [92–97]. Several fields including 3-D cell culturing have adapted the magnetically driven platforms [98–103]. An ability to create 3-D tumor spheroids that mimic *in vivo* tumors by utilizing a magnetic cell levitation method has been demonstrated [104]. Magnetic iron oxide (Fe_3O_4)-encapsulated poly(lactic-co-glycolide)(PLGA) micro-particles or poly(L-lactic acid)-*b*-poly (ethylene glycol)-folate [PLLA-*b*-PEG-folate] nanoparticles were utilized as substrates for 3-D tumor cell culture. The technique is based on the use of a simple, adaptable magnetic levitation of Fe_3O_4 nano-/micro-particles to achieve 3-D tumor structure (Fig. 4a). A similar methodology was adopted to generate 3-D tissue culture of human glioblastoma cells (Fig. 4b–d) [101]. The 3-

D cultured glioblastoma cells showed similar morphological and molecular characteristics to the orthotopic human xenografts from immunodeficient mice. The N-cadherin (a transmembrane protein mediating cell–cell contact) was expressed in the membrane, cytoplasm, and cell junctions, whereas in 2-D cultures the biomarker was dispersed in the nucleus and cytoplasm. The study utilized the magnetic levitation of cells in the presence of a hydrogel enclosing gold nanoparticles, magnetic iron oxide nano-particles, and filamentous bacteriophages during photo-crosslinking [93]. Although the applications of these magnetic nanoparticles (MNPs) loaded into the cell-encapsulated hydrogels (M-gel) have been utilized in tissue engineering, the possible interaction between the MNPs and encapsulated cellscan potentially affect their viability and functionality [93,94]. These MNPs can be released from biodegradable hydrogels in cultures overtime [105]. In alternating current magnetic field,the magnetic hyperthermia could affect the cells and lead to disassembly of the hydrogel as a result of accumulation of thermal energy inside the gels [95,106]. On other hand, in permanent magnetic field these adverse effects are not observed [95]. Although the FDA has approved the use of MNPs in several applications (e.g., imaging agent), further nanotoxicological studies would be vital for future applications including 3-D cell culture, drug testing, and regenerative medicine [93,107]. Recently, living soft materials were assembled by paramagnetic levitation-based approach (Fig. 5a and b) [95,108,109]. This approach manipulated cell seeded units (microgels and microbeads) in paramagnetic gadolinium-based medium for bottom-up tissue engineering. The microgels and microbeads were assembled in magnetic fields by their paramagnetic properties, without integrating them with other magnetic components (e.g., magnetic nanoparticles) [95,109]. This method is cost effective and as it does not require the expensive and potentially toxic MNPs. Furthermore, hydrogels can be assembled by non-magnetic methods using a micro-robotic system as recently demonstrated [96]. These untethered micro-robots are actuated by an external magnetic field and their motion can be controlled precisely to assemble 2-D and 3-D hydrogels encapsulating various types of cells (Fig. 5c). Alternatively, Faraday waves have been employed for liquid-based templated sound-based assembly of hydrogels and cells [110]. Topography of the liquid surface established by standing waves serves as a template for directed assembly of a large number of hydrogels quickly (in about 5 s) into diverse sets of ordered and symmetric structures (Fig. 5d). The assembled hydrogels can be immobilized by chemical- and photo-crosslinking for stable assembly. These hydrogel and cell assembly methodologies provide a new way of engineering 3-D constructs and present broad potential applications in regenerative medicine, drug screening, and experimental biology.

Basement membrane extract from mouse sarcoma

The basement membrane is a part of the ECM structure. It is composed of various proteins such as laminin, fibronectin, and collagen IV that are important for tissue growth and organization [111,112]. The basement membrane extract is routinely obtained from cancer cell cultures of mouse sarcoma (Engelbreth-Holm-Swam, EHS) and used for various applications in tissue engineering. The extracted EHS membrane extract is commercially available from different companies such as BD Matrigel™ and Trevigne Cultrex[1]. These membrane extracts resemble the natural tumor microenvironment and contain laminin (60%), collagen IV (30%), and entactin (8%). Various growth factors and hormones

including matrix metalloproteinase (MMP) enzymes that remodel ECM and promote cancer cell proliferation are also present [111,112]. When lung cancer cells were mixed in Matrigel and injected subcutaneously in an animal model, they rapidly formed a bigger tumor mass compared to injected cancer cells without Matrigel [113]. Other cancer cell lines such as A253 and B16F10 have also shown enhancement of cell growth rates (~5–10 times) when co-injected with Matrigel [113]. Furthermore, multicellular cultures can be obtained easily by mixing different cell types together with Matrigel. In one study, breast cancer cells and fibroblasts were mixed with Matrigel and co-cultured [114]. The grown tumor showed a more invasive response as fibroblast cells released MMP enzymes that reorganized the ECM [114]. Although the basement membrane extract is a powerful model to study the tumor behavior, it has a few limitations. Matrigel does not have high portions of collagen-I and hyaluronan that are usually present in high proportions in *in vivo* tumor microenvironments. These proteins play an important structural role in organizing tissue architecture. In the absence of these proteins, natural *in vivo* response of cancer cells may not be recapitulated in Matrigel [115]. The presence of unknown amount of other growth factors and proteins is another limitation associated with the use of Matrigel. The composition of Matrigel has batch to batch differences that have uncontrolled effects on cancer cell behavior [116]. As the composition of Matrigel cannot be controlled, the effect of a single hormone or growth factor on cancer cell behavior cannot be studied specifically. Despite these limitations, Matrigel is a natural gelatinous protein from mouse sarcoma cells and has found potential applications in the field of tumor growth and drug screening.

Hydrogel cellular scaffolds

Hydrogels are a crosslinked network of polymers and can absorb up to 99% of water because of their highly porous structure. Hydrogels are widely used in many cell culture and tissue engineering applications because of their high resemblance to physical structures of natural ECM [117,118]. Various natural and synthetic polymers are used for hydrogel synthesis. Examples of naturally occurring polymers and proteins used for hydrogel formations are collagen, hyaluronic acid, fibrin, silk protein, fibronectin, alginate, agarose, and chitosan [10,119–122]. Many of these natural substances are obtained from the mammalian ECM (hyaluronic acid, collagen and fibrin), whereas silk protein is obtained from silkworm [117,123]. Hydrogels made of natural polymers have been utilized in many cancer cell growth and proliferation studies [124,125]. In one study, three different populations of cells (luminal cells/MCF-7, myoepithelial cells and fibroblasts/tumor associated fibroblast) of breast tissue origin were mixed in a collagen hydrogel and allowed to grow over a period of 1 week [125]. Dual-cell co-units were formed with myoepithelial cells surrounding luminal cells (Fig. 6a(ii)). Cancer cells (MCF-7) and myoepithelial co-units both had disrupted basement membranes resembling *in vivo* ductal carcinoma *in situ* (DCIS), differentiating them from normal cell co-units [125]. Normal fibroblast cells had no effect on co-unit organization when cultured with luminal and myoepithelial cells, whereas the tumor associated fibroblast cells disrupted the co-units organization by releasing MMP enzymes (Fig. 6). Besides natural hydrogels, many synthetic hydrogels are also introduced in tissue engineering including Poly(hydroxyethyl methacrylate) (PHEMA), Poly(vinyl alcohol) (PVA), Poly(ethylene glycol) (PEG), Poly(acrylic acid) (PAA), Poly(methacrylic acid) (PMMA), and Poly(acrylamide) (PAAm) [117]. Synthetic hydrogels are also

commercially available such as self-assembling peptide hydrogel (RAD16-I) matrix (BD™ PuraMatrix™). Using hydro-gels, we can have a better control over the quantity of ECM proteins and growth factors, whereas basement membrane extract has non-quantified composition [116,126,127]. Ovarian cancer cells organized into an acinar shape when mixed with PuraMatrix hydrogel. The acinar shape resembled the *in vivo* cancer metastatic nodules [128]. PuraMatrix hydrogel was also functionalized with various motifs such as collagen, laminin and fibronectin. The addition of these functional motifs has been shown to increase the cell survival and attachment [129,130].

Polymeric scaffolds

Polymeric scaffolds are microporous structures with highly interconnected architecture similar to hydrogels. The main difference between polymeric scaffolds and hydrogels is that polymeric scaffolds are synthesized before cell seeding, whereas in hydrogel cells can be mixed with polymers before hydrogel formation [94,131]. Polymeric scaffolds are synthesized from natural (Collagen, Chitosan, Alginate) and synthetic polymers including PEG, polylactide (PLA), poly(lactide-co-glycolide) (PLG), polyglycolide (PGA), polystyrene, and poly(lactic-co-glycolic acid) (PLGA) [10,132–137]. Various polymeric scaffolds are commercially available in synthetic, non-degradable polystyrene (Alvetex by Reinnervate [138], 3-D insert PS by 3-D Biotek [139]) and natural degradable alginate forms (AlgiMatrix 3-D by Invitrogen) [140]. Polystyrene culture plates are routinely used for 2-D cell culture in laboratories. 3-D polystyrene based scaffold can be synthesized to get benefits of 3-D topography. In one report, lymph-node-derived HBL-2 cells showed increased growth rates when cultured in 3-D polystyrene scaffold as compared to 2-D polystyrene plates [139]. In another report, PLG synthetic scaffolds were used to study the behavior of tumor cells on these scaffolds. Oral squamous cell carcinoma (OSCC-3) and mouse Lewis Lung Carcinoma (LLC) cells were cultured on 3-D PLG scaffolds and 2-D culture plates then implanted into immunocompromised and immunocompe-tent mice, respectively [37]. The cancer cell growth was analyzed after 3 weeks. The OSCC-3 and LLC cancer cells pre-cultured on 3-D PLG scaffolds developed into larger tumor mass as compared to cells pre-cultured on 2-D plates (Fig. 7). The tumor cells pre-cultured on 3-D PLG scaffolds produced more angiogenic factors including the vascular endothelial growth factor (VEGF), basic fibroblast growth factor (bFGF), and IL-8 [37]. The increased level of angiogenic factors resulted in generation of more blood vasculature. 3-D porous chitosan-alginate (CA) based natural scaffold was synthesized for studying the prostate cancer cell–lymphocyte interactions [2]. Three different prostate cancer (PCa) cell lines (LNCaP, C4-2 and C4-2B) were cultured on 2-D culture plates, 3-D CA scaffolds, and in Matrigel for 15 days [2]. The cancer cells cultured on 2-D plates formed a flat layer of cells (Fig. 8). The Matrigel culture produced tumor spheroids, but the cells attached to the bottom plate surface formed flat and elongated shapes. All three cancer cell lines formed perfect spheres in the pores of 3-D CA scaffolds resembling the morphology of *in vivo* tumor mass (Fig. 8) [2]. These scaffolds also sustained the cancer cell growth for a longer period of time (55 days) without degradation, whereas Matrigel became highly degraded after one week. However, many polymeric synthetic scaffolds do not show good cellular attachment because of material properties such as type and degree of porosity. Enhanced cellular attachment is achieved by incorporating hydrophilic polymers (e.g., PVA and chitosan) into such synthetic scaffolds [141].

Incorporating ECM components in such synthetic scaffolds would enhance the cellular response *in vivo*.

Dynamic tumor models based on microfluidics

Microfluidic technologies allow precise control on small volumes of fluid inside channels and find numerous applications in disease diagnostics and medicine [142–147]. Various dynamic platforms based on microfluidic technologies have also been developed to model tumor microenvironment *in vitro* [148–151]. Microfluidic platforms allow a continuous supply of nutrients to growing cells, and have the ability to analyze the effects of shear stress on tumor cells [152,153]. In one study, a microfluidic platform was developed to study the effect of anti-cancer drug (Tegafur) on colon cancer cells while establishing multi-organ interactions [154]. The microfluidic platform was composed of three separate cell-hydrogel chambers containing colon cancer cells, hepatoma cells, and myeloblasts representing cancer, liver, and marrow, respectively. These cell-hydrogel chambers were connected with microfluidic channels mimicking blood flow. Using this device, researchers have successfully shown the metabolism of Tegafur in the liver chamber, followed by death of cancer cells by metabolic products. In another report, a dynamic microfluidic device was developed to analyze the albumin release from carcinoma cells embedded into peptide hydrogels [155]. The device also enabled chemotaxis studies by producing a gradient profile across carcinoma cells. Dynamic tumor platforms can be integrated with live-cell fluorescence microscopy to study the minute interactions between cancer and other cells such as endothelial cells forming blood vessels [156]. To study these interactions, a microfluidic platform was recently developed, which consists of an artificial blood vessel (lined with human umbilical vein endothelial cells) surrounded by breast cancer cells in ECM. Using this platform, scientists have shown the precise movement of breast cancer cells toward a vessel by forming a tunnel in ECM. Hence, these dynamic platforms can potentially be used in drug screening mimicking physiological environments, while reproducing multi-organ interactions.

Systems to model the effects of physical factors

The chemical, mechanical, and structural stimuli to mammalian cells in 3-D microenvironments in the human body change through the invasion and progression of a disease [157–160]. Through the course of cancer metastasis, cancer cells exfoliate from the primary solid tumor and enter the circulatory system of the patient to find an appropriate remote site to create a secondary tumor [161,162]. During this process, invasive cancer cells have to migrate through tiny pores in the 3-D ECM microenvironment [163–165]. Therefore, investigating the physical interaction between the invasive cancer cells and their 3-D microenvironments as well as their cellular response physical factors (i.e., ECM stiffness, flow, and shear stress) can lead to a better understanding of cancer metastasis mechanisms [165–169]. For instance, cancer cell migration has been investigated in spatially 3-D gradient microenvironments using polydimethylsiloxane (PDMS) tapered microchannels that connect a wide microchannel (4 μm × 10 μm) to a narrow microchannel (15 μm × 10 μm). This study revealed how cancer cells migrated from a more confined environment (narrow channels) to a region with greater amounts of freedom (wide channels). Highly

metastatic breast cancer cells (MDA-MB-231) migrated through the tiny microchannels in a PDMS device, whereas non-metastatic breast cancer cells (MCF-10A) showed less invasiveness, as they could not migrate through the narrow channels [165].

Cancer cell response to matrix stiffness

Matrix stiffness is another important parameter in studying the cellular response of cancer cells in 3-D microenvironment [170]. The matrix stiffness of different body organs can be quantified by Young's modulus (E) that can be soft as brain tissue (250–500 Pa) or rigid as bone (1–25 GPa) [159,171]. Cellular mechanical response in these microenvironments with different degrees of ECM mechanical stiffness is different. Matrix stiffness of solid tumors changes during the course of cancer metastasis and progression [157,172]. For instance, breast tumor has shown a stiffer microenvironment (4000 Pa) compared to the healthy breast tissue (200 Pa) [157]. One of the most popular and effective protein hydrogels that has been used to investigate cancer cell response to 3-D matrixes with different stiffness is collagen hydrogels [157,159,173]. The stromal collagen deposition and crosslinking can define the stiffness of the tumor microenvironment and consequently can alter the cancer cell migration through the ECM [173]. In one report, a substrate with varying stiffness was synthesized using polyacrylamide hydrogel and cells migrated from a soft substrate to a stiffer substrate [174]. This study showed that the cells grown on stiffer substrates had longer contact lengths. In another investigation, metastatic cancer cells were characterized by measuring the traction forces applied to 2-D and 3-D matrixes *via* cancer cells on these substrates [175]. Breast, lung, and prostate cancer cells showed significantly stronger traction forces on the substrate at the late stage of the cancer disease compared to the normal healthy cells. Further, these results showed that cancer cells created stronger contractile forces on matrixes with higher stiffness. The degrees of the traction and contraction forces generated by cancer cells are determined by the chemical and mechanical properties of tumor microenvironment [8,175].

Cellular response to fluid shear stress

In addition to the matrix stiffness, fluid shear stress in the 3-D microenvironment inside the ECM is another critical extracellular stimulus that modulates MMP genes [176]. The ECM structure surrounding the solid tumor is degraded during the very first stage of metastasis because of matrix MMPs [177–179]. In this case, shear forces on the cancer cells exfoliating from the primary tumor can potentially change the mechanical response and migration of invasive cancer cells entering into the circulatory system [176]. To verify this phenomenon, a recent study has investigated the effect of shear stresson cell migration [179]. Inthisstudy, fluid flow and shear stress on the cancer cells changed the migratory response of the cancer cells by reducingtheir motility because of changing the level of MMP expression in the microenvironment [179]. The results explained why the glioma cells *in vitro* had different invasiveness compared to *in vivo* [179]. In another instance, researchers have investigated the role of fluidic shear forces in cancer metastatic biology in a micro-fluidic platform using 3-D ovarian cancer nodules [28]. They observed that the fluidic shear forces induce aggressive tumor phenotype by posttranslational up-regulation of EGFR and vimentin, and down-regulation of E-cadherin protein expression [28].

Cancer cell response to host immune modulatory effect

The development, growth, invasion, and treatment of cancers are clearly influenced by the interaction of tumor cells with immune system. Culturing these cells in 2-D has enabled discovery of new drugs and has allowed for a better understanding of cancer patho-physiology. However, these 2-D cultures are still unable to recapitulate the 3-D tumor microenvironment, resulting in wide discrepancies between immunotherapy data obtained from *in vitro* experiments and clinical trials [180,181]. In addition, although animal models have been useful in evaluating tumorigenic potential of cancer cells, these models lack the same tumor and immune system interactions present in humans, because tumor cells in these models are cultured in complete or partial absence of immune cells and immune modulatory chemical factors such as cytokines, and in the presence of the animal stromal cells and matrix [180,182,183]. Therefore, modulating the tumor and immune system interactions in 3-D cultures can be of great importance for successfully evaluating cancer immunotherapy and drug screening. Recent studies have integrated immune cells in 3-D culture to study their association with tumors, aiming to develop better *in vitro* models for drug testing and experimental cancer biology [184,185]. For instance, macrophages (which are usually recruited by solid tumors during their progression) were integrated into a collagen-based 3-D co-culture system of squamous cell carcinoma (SCCs) [185]. The study demonstrated that M2 polarized populations of macrophages have tumor-promoting effects. This approach, which established a complex human 3-D model system for skin SCCs, has the potential to explore the activation of macrophages in human systems during cancer progression. In a similar study, melanoma cells cultured in spheroids showed immunomodulator functions in addition to inhibition of mitogen-dependent T-lymphocyte activation and proliferation, which suggests an important role of spheroids in evading immune surveillance [184]. This approach provides a useful model to study the aggressiveness of certain malignancies and can be utilized to investigate the poor responses of malignancies to various immunotherapy drug treatments. Furthermore, modulating the tumor microenvironment to favor the presence of pro-inflammatory cytokines has been shown to enhance the immune response by promoting immune cell migration and activation [186]. For example, the expression of chemokine ligand 21 (CCL21) and interferon gamma (IFNγ) in a breast cancer 3-D model demonstrated the ability to enhance T cell recruitment and activation in the tumor [187]. Overall, the ability of a 3-D culture system with the addition of immune cells or immune factors to better mimic tumor microenvironments would potentially develop new platforms for cancer therapy.

Imaging 3-D cultures in living animals

It is clear from the literature that 3-D cultures are able to control and produce precise microenvironment that is more similar to human tissues. The microenvironment can also be modified by the use of various biomaterials with specific properties as discussed in previous sections. The animal models implanted with xenograft of cells grown in 3-D scaffolds with human tissue microenvironment can add another dimension by providing a more similar *in vivo* model system to study human cancers for drug testing, evaluating metastasis and invasive profile of cancer cells, and also in various cell therapy studies for cardiac and islet transplantation. Currently, noninvasive small animal imaging provides the advantage of

monitoring various properties of cells implanted within scaffolds in intact live animals over time without sacrificing them. Bioluminescence imaging, fluorescence imaging, X-ray assisted computer tomography imaging (CT), and magnetic resonance imaging (MRI) offers imaging cells implanted in 3-D scaffolds with or without pre-labeling. Adipose-derived progenitor cells (ADPC) dually labeled with bioluminescent (Firefly luciferase) and fluorescent (GFP) reporter genes cultured in a combination of porous elastomeric membrane and peptide hydrogel, were evaluated as a bio-implant for cardiac regeneration in a mouse model of myocardial infarction [188]. As ADPC expresses reporter genes, the viability and function of cells can be monitored by imaging and can also be compared with the improvements in cardiac function. The results of this study showed a well-adapted bioactive implant to the heart, and developed fully functional vessels across the myocardium and bioactive implant interface. The results also achieved significant improvement in the cardiac function, as revealed by echocardiography. Similarly, in another study various 3-D culture systems, such as Porous Polycaprolactone Scaffold (Kiyatec), Hyaluronic Acid Gel (Celenys), Magnetic Levitation Bioassembler (n3D Biosciences), and UV Cross-linked Poly-ethylene Glycol Hydrogel were developed to mimic human *in vivo* condition similar to ECM, and study the conditions using cells pre-labeled to express bacterial luciferase (*lux* gene) by bioluminescence imaging [189]. This study tested the system under various conditions, such as growth temperature, time period and antibiotic treatment response, and the results showed the bioluminescence imaging can feasibly differentiate the response of cells in a 3-D culture system under various conditions.

MRI is a high resolution imaging technique routinely used for various diagnostic applications including cancer. MRI is used in combination with various contrast agents for cell tracking in stem cells studies. Adipose Derived Stem Cells (ADSCs) isolated from human tissues labeled with Ultrasmall Super Paramagnetic Iron Oxide (USPIO) particles seeded within a 3-D porous polysaccha-ride-scaffold were subcutaneously implanted in animals for tissue engineering and monitored by MRI over time [190]. The USPIO labeling of cells did not affect the viability and differentiation potential of ADSCs. The *in vivo* imaging in animals showed the presence of viable cells even 28 days after implantation and cells migrated and colonized around the scaffold. Similarly, in another study, three different structures with tunable architectures prepared from naturally occurring polysaccharides were explored as scaffolds for mesenchymal stem cell (MSC) culture using a 1.5T high resolution MRI. The study used anionic citrate coated iron oxide nanoparticles as MR contrast agents to label MSCs. *In vivo* imaging of MSC in 3-D scaffolds clearly detected the architecture of the scaffolds [191]. Although the development of 3-D culture system for various applications has been widely studied [192], the feasibility of imaging 3-D scaffolds in animal models for long-term functional evaluations is still limited.

Future research directions and concluding remarks

3-D cancer models recapitulate native tumor environment compared to monolayer cultures and standardization and automation of 3-D tumor models are needed for broad applications. Although hundreds of thousands of spheroids can be synthesized using bio-printing and hanging drop methods, there are concerns about production efficiency and spheroid size uniformity. Variations in spheroid size affect the uniform diffusion of nutrients inside the

core and, hence uneven cell growth was observed in individual spheroids [193]. In the case of scaffold based 3-D models, the nature of scaffold material affects the absorption and adhesion of the drugs that are being tested [194]. The scaffold and materials should be carefully selected based on the nature of screening drugs and their interactions with various materials [195,196]. Although 3-D tumor models allow co-culture of various cell types mimicking tumor environment, an exhaustive set of experiments need to be designed to analyze the effect of each cell population on others. Various cell types will require different culture conditions; one culture medium may not be effective for all cell types. The requirement of maintaining specific growth conditions for various cell types inside a 3-D tumor model may require complex peripheral component design. The effect of ratio of a specific cell type to other cells in a co-culture environment should also be thoroughly explored and experiments should be performed to not only analyze commonly tested parameters such as cell growth and invasiveness, but genetic and epigenetic changes should be analyzed over a period of time. 3-D tumor models showing promising results during exhaustive cross-pharma validations could potentially be adopted by pharmaceutical industry.

3-D tumor models should be capable of automated readout and imaging [197]. The image analysis of cancer cells in 3-D cultures is often limited by autofluorescence of scaffold material such as collagenous scaffolds. Cancer cells encapsulated into 3-D tumor models need to be recovered for further biochemical and cell analysis. Methods are lacking for gentle recovery of growing cancer cells from non-degradable scaffolds such as polystyrene based synthetic scaffolds. Researchers have synthesized PLG based 3-D scaffolds that can be degraded enzymatically to release cultured cancer cells without affecting them [37]. In one recent report, a porous 3-D collagen-alginate scaffold was synthesized and degraded by the addition of ionic solution. The polyelectrolyte complex between alginate and collagen was disrupted by the ionic solution leading to degradation of 3-D scaffolds and release of cancer cells [2]. Similar methodologies should be adapted for other 3-D scaffold models. Although the scaffold-free 3-D tumor models are considered more compatible with automation, they have uncontrolled composition and batch-to-batch variation (basement membrane extract). One way to standardize the 3-D model composition is to allow the stromal cells to deposit their own basement membrane extract before cancer cells are further cultured [197]. Furthermore, the capability of co-culturing the patient’s own cancer, immune, and stromal cells to generate 3-D tumor models would truly personalize cancer therapy and create a new area in precision medicine. This approach would allow to develop a new line of effective and customized drugs that are targeting specifically the patient’s own cancer cells. In addition, this approach has the potential to minimize the side effects associated with drug screening using conventional drug testing methods. The future is promising for such approaches, where the patient’s life is prolonged and quality of their health is maintained.

Acknowledgments

We would like to thank Shuqi Wang and Fatih Inci for their feedback and Pu Chen for his help in making Fig. 4. We also thank Hassan Sakhta as a high school student under the Student Success Job Program at Brigham and Women’s Hospital (BWH), Sedef Dalbeyler as a summer intern at BWH, Mudit Tandon from Belmont Hill High School, as well as Srikar Srivatsa from Cupertino High School for contributing in drawing the schematic figures.

We thank Jedediah Lewis, a doctoral student in Stanford University's Biosciences Program and BAMM Labs at Stanford for his feedback on the manuscript. We would also like to thank research support from College of Engineering and Computer Science, Florida Atlantic University. This work was supported by NSF CAREER 1150733, NIH R15HL115556, NIH R21HL112114, NIH R01EB015776, NIH F32AI102590, the Brigham and Women's Hospital Bright Futures Award, and the Brigham and Women's Hospital Innovation Evergreen Fund.

References

1. Bissell MJ, Radisky D. Cancer. 2001; 1(1):46. [PubMed: 11900251]
2. Florczyk SJ, et al. Adv Healthcare Mater. 2012; 1(5):590.
3. Asghar, W., et al. Cancer Targeted Drug Delivery. Springer; 2013. In vitro three-dimensional cancer culture models; p. 635
4. Shin CS, et al. Mol Pharm. 2013; 10(6):2167. [PubMed: 23461341]
5. Krausz E, et al. J Biomol Screen. 2013; 18(1):54. [PubMed: 22923784]
6. Hui EE, Bhatia SN. Proc Natl Acad Sci USA. 2007; 104(14):5722. [PubMed: 17389399]
7. Polacheck WJ, et al. Cell Mol Life Sci. 2013; 70(8):1335. [PubMed: 22926411]
8. Shi Q, et al. Proc Natl Acad Sci USA. 2014; 111(2):658. [PubMed: 24379367]
9. Alberts, B., et al. Molecular Biology of the Cell. Garland Science; New York: 2002.
10. Geckil H, et al. Nanomedicine. 2010; 5(3):469. [PubMed: 20394538]
11. D'Antonio G, et al. Math Biosci Eng. 2012; 10:75.
12. Tibbitt MW, Anseth KS. Biotechnol Bioeng. 2009; 103(4):655. [PubMed: 19472329]
13. Wang L, et al. Nano Today. 2013; 8(4):374.
14. Schreiber RD, et al. Sci Signal. 2011; 331(6024):1565.
15. Vesely MD, et al. Annu Rev Immunol. 2011; 29:235. [PubMed: 21219185]
16. Romero P, et al. Immunotherapy. 2004; 53(3):249.
17. Hortobagyi GN. Semin Oncol. 2004; 31:21.
18. Cheever MA, Higano CS. Clin Cancer Res. 2011; 17(11):3520. [PubMed: 21471425]
19. Abbott A. Nature. 2003; 424(6951):870. [PubMed: 12931155]
20. Cekanova M, Rathore K. Drug Des Dev Ther. 2014; 8:1911.
21. Ellem SJ, et al. Adv Drug Deliv Rev. 2014
22. Choi SYC, et al. Adv Drug Deliv Rev. 2014
23. Sung KE, Beebe DJ. Adv Drug Deliv Rev. 2014
24. Kimlin L, et al. Expert Opin Drug Discov. 2013; 8(12):1455. [PubMed: 24144315]
25. Thoma CR, et al. Adv Drug Deliv Rev. 2014; 69:29. [PubMed: 24636868]
26. Seo BR, et al. Adv Drug Deliv Rev. 2014; 69:205. [PubMed: 24309015]
27. Håkanson M, et al. Adv Drug Deliv Rev. 2014; 69:52. [PubMed: 24295904]
28. Rizvi I, et al. Proc Natl Acad Sci USA. 2013; 110(22):E1974. [PubMed: 23645635]
29. Celli JP, et al. J Biomed Opt. 2010; 15(5):051603. [PubMed: 21054077]
30. Hammer E, et al. Proteomics. 2010; 10(1):99. [PubMed: 20017144]
31. Luca AC, et al. PLoS ONE. 2013; 8(3):e59689. [PubMed: 23555746]
32. Bellis SL. Biochim Biophys Acta: Biomembr. 2004; 1663(1):52.
33. Benton G, et al. J Cell Physiol. 2009; 221(1):18. [PubMed: 19492404]
34. SHIN C, et al. Biomaterials for Cancer Therapeutics: Diagnosis, Prevention and Therapy. 2013:445.
35. Wang F, et al. Proc Natl Acad Sci USA. 1998; 95(25):14821. [PubMed: 9843973]
36. dit Faute MA, et al. Clin Exp Metastasis. 2002; 19(2):161. [PubMed: 11964080]
37. Fischbach C, et al. Nat Methods. 2007; 4(10):855. [PubMed: 17767164]
38. DelNero P, et al. Biomaterials. 2015; 55:110. [PubMed: 25934456]
39. Elliott NT, Yuan F. J Pharm Sci. 2011; 100(1):59. [PubMed: 20533556]
40. Deisboeck TS, et al. Annu Rev Biomed Eng. 2011:13.

41. Xu F, et al. Biofabrication. 2011; 3(3)
42. Richmond A, Su Y. Dis Mod Mech. 2008; 1(2–3):78.
43. Chan CT, et al. Cancer Res. 2014 (canres. 0138.2014).
44. Becher OJ, Holland EC. Cancer Res. 2006; 66(7):3355. [PubMed: 16585152]
45. Wilkosz S, et al. Anat Embryol (Berl). 2005; 209(3):251. [PubMed: 15662530]
46. Voskoglou-Nomikos T, et al. Clin Cancer Res. 2003; 9(11):4227. [PubMed: 14519650]
47. Day CP, et al. Int J Cancer. 2012; 130(1):190. [PubMed: 21312195]
48. Smalley KS, et al. In Vitro Cell Dev Biol Anim. 2006; 42(8–9):242. [PubMed: 17163781]
49. Sun P, et al. Oncol Lett. 2013; 5(2):489. [PubMed: 23420461]
50. Tang J, et al. Tumour Biol. 2011; 32(3):469. [PubMed: 21140254]
51. Li X, et al. Nat Med. 2014; 20(7):769. [PubMed: 24859528]
52. Seib FP, et al. Biomaterials. 2015; 51:313. [PubMed: 25771021]
53. Becker-Weimann S, et al. Oncotarget. 2013; 4(11):2010. [PubMed: 24243820]
54. Nyga A, et al. Acta Biomater. 2013; 9(8):7917. [PubMed: 23624217]
55. Kunz-Schughart LA, et al. Am J Physiol: Cell Physiol. 2006; 290(5):C1385. [PubMed: 16601149]
56. Friedrich J, et al. Nat Protoc. 2009; 4(3):309. [PubMed: 19214182]
57. Tung YC, et al. Analyst. 2011; 136(3):473. [PubMed: 20967331]
58. Kunz-Schughart LA, et al. J Biomol Screen. 2004; 9(4):273. [PubMed: 15191644]
59. Chan HF, et al. Sci Rep. 2013:3.
60. Lin RZ, Chang HY. Biotechnol J. 2008; 3(9–10):1172. [PubMed: 18566957]
61. Hsiao AY, Kuo TY, Mosadegh CH, Bedenis B, Pienta R, Takayama KJS. Biomed Microdevices. 2012; 14(2):313. [PubMed: 22057945]
62. Torisawa YS, et al. Lab Chip. 2007; 7(6):770. [PubMed: 17538720]
63. Ungrin MD, et al. PLoS ONE. 2008; 3(2):e1565. [PubMed: 18270562]
64. Lee WG, et al. C Tissue Eng Part, Methods. 2010; 16(2):249.
65. Toh YC, et al. Lab Chip. 2007; 7(3):302. [PubMed: 17330160]
66. Fukuda J, Yeo KA, Yang Y, Yeh X, Eng J, Blumling G, Wang J, Kohane CF, Langer DSR. Biomaterials. 2006; 27(30):5259. [PubMed: 16814859]
67. Hsiao AY, et al. Biotechnol Bioeng. 2012; 109(5):1293. [PubMed: 22161651]
68. Xu F, et al. Biomicrofluidics. 2011; 5(2):022207.
69. Tasoglu S, Demirci U. Trends Biotechnol. 2013; 31(1):10. [PubMed: 23260439]
70. Xu F, et al. Biotechnol J. 2010; 6:204.
71. Moon S, et al. PLoS ONE. 2011; 6(3):e17455. [PubMed: 21412416]
72. El Assal R, et al. Adv Mater. 2014; 26(33):5815. [PubMed: 25047246]
73. Asghar W, et al. Biotechnol J. 2014; 9(7):895. [PubMed: 24995723]
74. Gurkan UA, et al. Mol Pharm. 2014
75. Gurkan U, et al. J Tissue Eng Regen Med. 2012; 6:366.
76. Visconti RP, et al. Expert Opin Biol Ther. 2010; 10(3):409. [PubMed: 20132061]
77. Mironov V, et al. Biomaterials. 2009; 30(12):2164. [PubMed: 19176247]
78. Boland T, et al. Biotechnol J. 2006; 1(9):910. [PubMed: 16941443]
79. Yanez M, et al. Tissue Eng A. 2014; 21(1–2):224.
80. Zhang T, et al. Biofabrication. 2013; 5(4):045010. [PubMed: 24280635]
81. El Assal R, et al. Nanomed (Lond Engl). 2015; 10(3):347.
82. Moon S, et al. Tissue Eng C: Methods. 2010; 16(7):157.
83. Ceyhan E, et al. Lab Chip. 2012; 12(22):4884. [PubMed: 23034772]
84. Zhao Y, et al. Biofabrication. 2014; 6(3):035001. [PubMed: 24722236]
85. Nakamura M, et al. Tissue Eng. 2005; 11(11–12):1658. [PubMed: 16411811]
86. Odde DJ, Renn MJ. Trends Biotechnol. 1999; 17(10):385. [PubMed: 10481169]
87. Nahmias Y, Odde DJ. Nat Protoc. 2006; 1:2288. [PubMed: 17406470]

88. Xu T. Biomaterials. 2005; 26:93. [PubMed: 15193884]
89. Xu T. Biomaterials. 2006; 27:3580. [PubMed: 16516288]
90. Demirci U, Montesano G. Lab Chip. 2007; 7(9):1139. [PubMed: 17713612]
91. Demirci U. J Microelectromech Syst. 2006; 15(4):957.
92. Sekeroglu K, et al. Appl Phys Lett. 2011; 99(6):63703. [PubMed: 21901051]
93. Xu F, et al. Adv Mater. 2011; 23(37):4254. [PubMed: 21830240]
94. Gurkan UA, et al. Adv Healthcare Mater. 2012; 1(2):149.
95. Tasoglu S, et al. Adv Mater. 2013; 25(8):1137. [PubMed: 23288557]
96. Tasoglu S, et al. Nat Commun. 2014:5.
97. Guven S, et al. Trends Biotechnol. 2015
98. Frasca G, et al. Langmuir. 2009; 25(4):2348. [PubMed: 19166275]
99. Yellen BB, et al. Proc Natl Acad Sci U S A. 2005; 102(25):8860. [PubMed: 15956215]
100. Kose AR, et al. Proc Natl Acad Sci U S A. 2009; 106(51):21478. [PubMed: 19995975]
101. Souza GR, et al. Nat Nanotechnol. 2010; 5(4):291. [PubMed: 20228788]
102. Mirica KA, et al. Adv Mater. 2011; 23(36):4134. [PubMed: 21830239]
103. Krebs MD, et al. Nano Lett. 2009; 9(5):1812. [PubMed: 19326920]
104. Lee WR, et al. Colloids Surf B: Biointerfaces. 2011; 85(2):379. [PubMed: 21420837]
105. Xu F, et al. ACS Nano. 2012; 6(8):6640. [PubMed: 22680777]
106. Le Renard PE, et al. Biomaterials. 2010; 31(4):691. [PubMed: 19878991]
107. LaConte L, et al. Mater Today. 2005; 8(5):32.
108. Tasoglu S, et al. Adv Healthcare Mater. 2015
109. Rodell CB, Burdick JA. Nature. 2014; 514(7524):574. [PubMed: 25355357]
110. Chen P, et al. Adv Mater. 2014; 26(34):5936. [PubMed: 24956442]
111. Kleinman HK, Martin GR. Semin Cancer Biol. 2005; 15:378. [PubMed: 15975825]
112. Kleinman HK, et al. Biochemistry. 1986; 25(2):312. [PubMed: 2937447]
113. Webber MM, et al. Carcinogenesis. 1997; 18(6):1225. [PubMed: 9214606]
114. Shekhar MPV, et al. Cancer Res. 2001; 61(4):1320. [PubMed: 11245428]
115. Nyga A, et al. J Cell Commun Signal. 2011; 5(3):239. [PubMed: 21499821]
116. Gelain F, et al. PLoS ONE. 2006; 1(1):e119. [PubMed: 17205123]
117. Peppas NA, et al. Adv Mater. 2006; 18(11):1345.
118. Hutmacher DW, et al. Trends Biotechnol. 2010; 28(3):125. [PubMed: 20056286]
119. Kwon H, et al. J Tissue Eng Regen Med. 2010; 4(8):590. [PubMed: 20865693]
120. Cheng SY, et al. Cytotechnology. 2006; 51(3):159. [PubMed: 19002886]
121. Zhang T, et al. J Tissue Eng Regen Med. 2012; 6(9):748. [PubMed: 22081518]
122. Mohammadi H, et al. Biomaterials. 2014; 35(4):1138. [PubMed: 24215732]
123. Mandal BB, Kundu SC. Biotechnol Bioeng. 2008; 99(6):1482. [PubMed: 17969177]
124. Neel EAA. Soft Matter. 2006; 2(11):986.
125. Holliday DL, et al. Breast Cancer Res. 2009; 11(1):R3. [PubMed: 19152687]
126. Spancake KM, et al. Cancer Res. 1999; 59(24):6042. [PubMed: 10626787]
127. Albrecht DR, et al. Nat Methods. 2006; 3(5):369. [PubMed: 16628207]
128. Adnan OA-Y, et al. J Vis Exp. 2009; 34
129. Kisiday J, et al. Proc Natl Acad Sci USA. 2002; 99(15):9996. [PubMed: 12119393]
130. Davis ME, et al. Circulation. 2005; 111(4):442. [PubMed: 15687132]
131. Guven S, et al. Trends Biotechnol. 2015; 33(5):269. [PubMed: 25796488]
132. Buurma B, et al. Eur J Oral Sci. 2003; 107(4):282.
133. Asghar W, et al. IEEE Trans Nanotechnol. 2012; 11(3):546.
134. Ilyas A, et al. IEEE Trans Nanotechnol. 2013; 12(6):1082.
135. Asghar W, et al. Nanotechnology. 2012; 23(47):475601. [PubMed: 23111337]
136. Traore MA, Behkam B. J Micromech Microeng. 2013; 23(8):085014.

137. Trachtenberg JE, et al. J Biomed Mater Res A. 2014; 102(12):4326. [PubMed: 25493313]
138. Knight E, et al. Methods Mol Biol (Clifton, NJ). 2011; 695:323.
139. Caicedo-Carvajal CE, et al. J Tissue Eng. 2011; 2(1)
140. Elkayam T, et al. Tissue Eng. 2006; 12(5):1357. [PubMed: 16771648]
141. Sahoo SK, et al. Biomacromolecules. 2005; 6(2):1132. [PubMed: 15762686]
142. Shafiee H, et al. Sci Rep. 2015:5.
143. Ilyas A, et al. Biosens Bioelectron. 2014; 62:343. [PubMed: 25038540]
144. Asghar W, et al. Adv Healthcare Mater. 2014; 3(10):1671.
145. Ilyas A, et al. Anal Methods. 2014; 6(18):7166.
146. Islam M, et al. Br J Med Med Res. 2014; 4(11):2129.
147. Guven S, et al. Stem Cells Transl Med. 2015; 4(3):261. [PubMed: 25666845]
148. Jeon JS, et al. Proc Natl Acad Sci USA. 2015; 112(1):214. [PubMed: 25524628]
149. Kim C, et al. Lab Chip. 2015; 15(1):301. [PubMed: 25370780]
150. Jin S, Ye K. Rec Patents Anti-cancer Drug Discov. 2013; 8(2):143.
151. Dash A, et al. Am J Physiol: Cell Physiol. 2013; 304(11):C1053. [PubMed: 23485712]
152. Giese C, Marx U. Adv Drug Deliv Rev. 2014; 69:103. [PubMed: 24447895]
153. Sei Y, et al. Microfluid Nanofluid. 2014; 16(5):907.
154. Sung JH, Shuler ML. Lab Chip. 2009; 9(10):1385. [PubMed: 19417905]
155. Kim MS, et al. Biomed Microdevices. 2007; 9(1):25. [PubMed: 17103048]
156. Wong AD, Searson PC. Cancer Res. 2014; 74(17):4937. [PubMed: 24970480]
157. Paszek MJ, et al. Cancer Cell. 2005; 8(3):241. [PubMed: 16169468]
158. Conklin MW, et al. Am J Pathol. 2011; 178(3):1221. [PubMed: 21356373]
159. Kraning-Rush CM, Reinhart-King CA. Cell Adhes Migr. 2012; 6(3):274.
160. Michor F, et al. Nat Rev Cancer. 2011; 11(9):657. [PubMed: 21850037]
161. Chaffer CL, Weinberg RA. Science. 2011; 331(6024):1559. [PubMed: 21436443]
162. Asghar W, et al. Lab Chip. 2012; 12(13):2345. [PubMed: 22549275]
163. Chambers AF, et al. Nat Rev Cancer. 2002; 2(8):563. [PubMed: 12154349]
164. Sahai E. Nat Rev Cancer. 2007; 7(10):737. [PubMed: 17891189]
165. Mak M, et al. PLoS ONE. 2011; 6(6):e20825. [PubMed: 21695222]
166. Mahler GJ, et al. Biotechnol Bioeng. 2014; 111(11):2326. [PubMed: 24898772]
167. Dai G, et al. J Biomech Eng. 1999; 121(6):557. [PubMed: 10633254]
168. Ozdemir T, et al. Am J Physiol: Cell Physiol. 2012; 302(8):C1189. [PubMed: 22262064]
169. Provenzano PP, Keely PJ. J Cell Sci. 2011; 124(8):1195. [PubMed: 21444750]
170. Chauhan VP, et al. Cancer Cell. 2014; 26(1):14. [PubMed: 25026209]
171. Zysset PK, et al. J Biomech. 1999; 32(10):1005. [PubMed: 10476838]
172. Levental KR, et al. Cell. 2009; 139(5):891. [PubMed: 19931152]
173. Carey SP, et al. Biomaterials. 2012; 33(16):4157. [PubMed: 22405848]
174. Charest JM, et al. Macromol Biosci. 2012; 12(1):12. [PubMed: 22021131]
175. Kraning-Rush CM, et al. PLoS ONE. 2012; 7(2):e32572. [PubMed: 22389710]
176. Binder DK, Berger MS. J Neurooncol. 2002; 56(2):149. [PubMed: 11995816]
177. Ramanujan S, et al. Biophys J. 2002; 83(3):1650. [PubMed: 12202388]
178. Hegedus B, et al. Biophys J. 2006; 91(7):2708. [PubMed: 16829558]
179. Qazi H, et al. PLoS ONE. 2011; 6(5):e20348. [PubMed: 21637818]
180. Hirt C, et al. Adv Drug Deliv Rev. 2014; 79:145. [PubMed: 24819215]
181. Feder-Mengus C, et al. Trends Mol Med. 2008; 14(8):333. [PubMed: 18614399]
182. Junttila MR, de Sauvage FJ. Nature. 2013; 501(7467):346. [PubMed: 24048067]
183. Singh M, Ferrara N. Nat Biotechnol. 2012; 30(7):648. [PubMed: 22781694]
184. Ramgolam K, et al. PLoS ONE. 2011; 6(4):e18784. [PubMed: 21526207]
185. Linde N, et al. PLoS ONE. 2012; 7(7):e40058. [PubMed: 22792213]

186. Kaufman HL, Disis ML. J Clin Invest. 2004; 113(5):664. [PubMed: 14991063]
187. Phan-Lai V, et al. Anti-Cancer Agents Med Chem. 2014; 14(2):204.
188. Soler-Botija C, et al. Am J Transl Res. 2014; 6(3):291. [PubMed: 24936221]
189. Webb JD. University of Tennessee Honors Thesis Projects. 2014:1.
190. Lalande C, et al. Eur Cell Mater. 2011; 21:341. [PubMed: 21484704]
191. Poirier-Quinot M, et al. Tissue Eng C: Methods. 2010; 16(2):185.
192. Wilson RH, et al. J Biomed Opt. 2015; 20(3):030901. [PubMed: 25803186]
193. Smalley KS, et al. Expert Opin Drug Discov. 2008; 3(1):1–10. [PubMed: 23480136]
194. Nugraha B, et al. Biomaterials. 2011; 32(29):6982. [PubMed: 21741702]
195. Roth A, Singer T. Adv Drug Deliv Rev. 2014; 69:179. [PubMed: 24378580]
196. Schimek K, et al. Lab Chip. 2013; 13(18):3588. [PubMed: 23743770]
197. Smalley KSM, et al. Expert Opin Drug Discov. 2008; 3(1):1. [PubMed: 23480136]

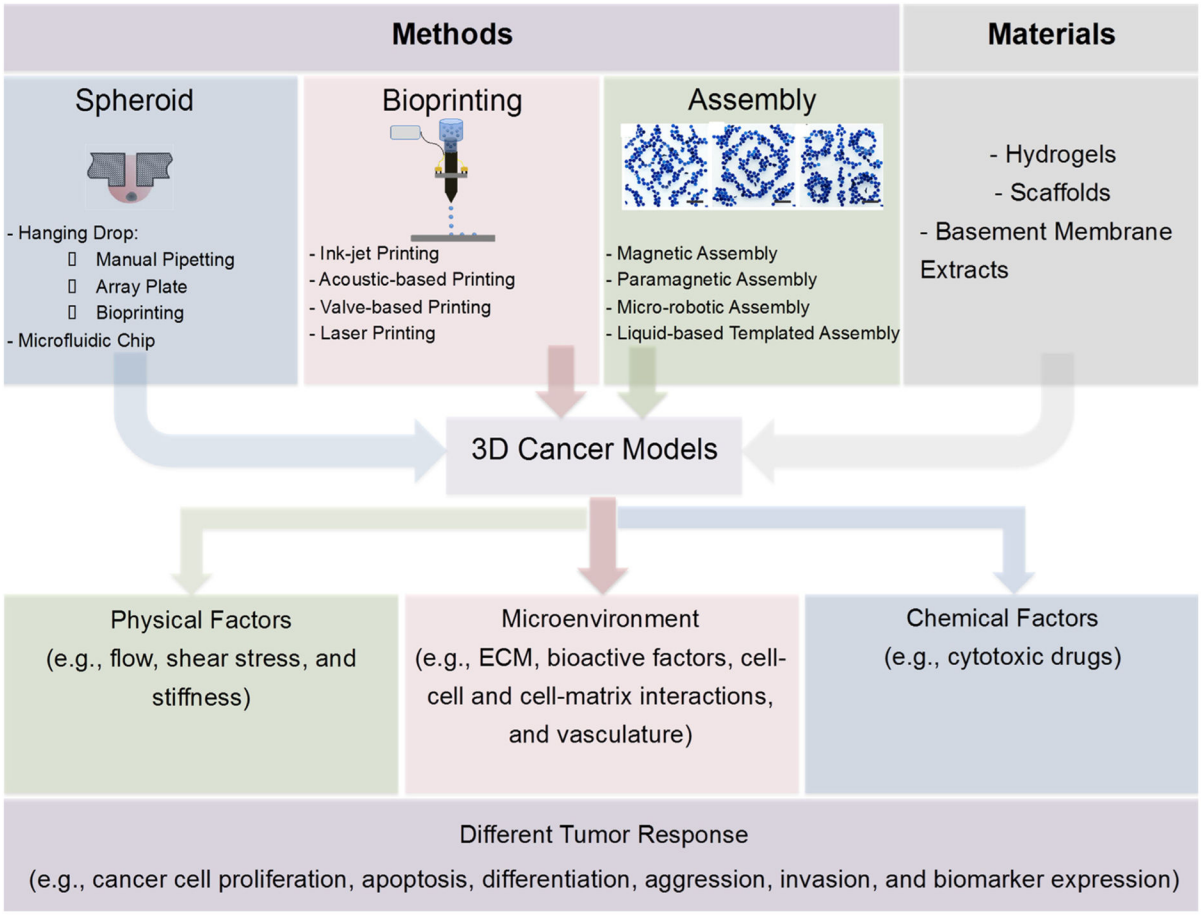

FIGURE 1.

Methods and materials used to engineer 3-D cancer models. To generate 3-D cancer models various technologies are used including spheroids, bio-printing, and assembly. These technologies are implemented using numerous kinds of materials such as hydrogels, scaffolds, and basement membrane extracts. Controlling physical and chemical factors and mimicking the native microenvironment results in tumor responses such as cancer cell proliferation, aggression, and invasion.

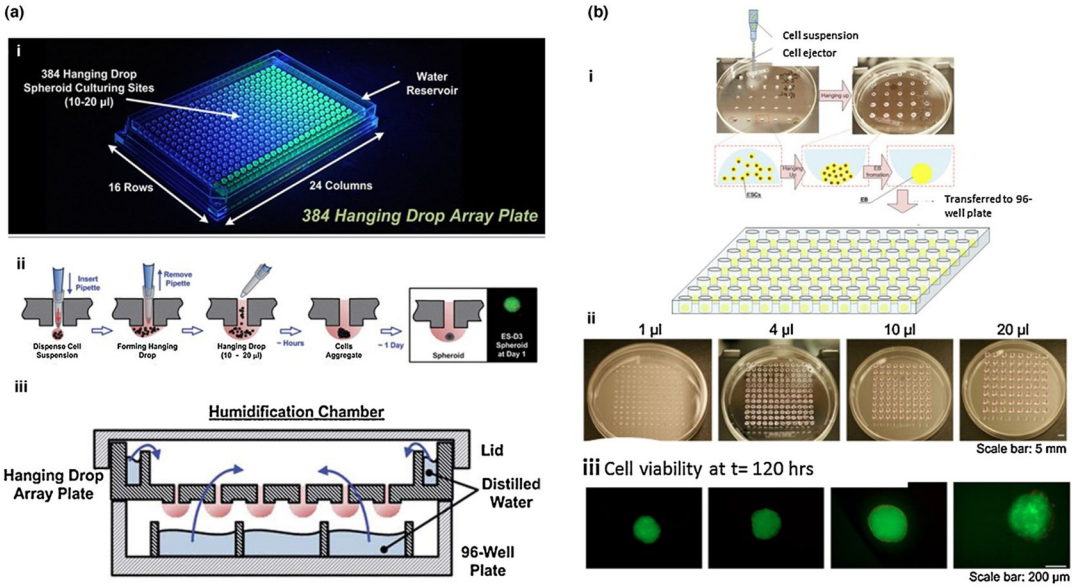

FIGURE 2.

High throughput methods to generate spheroids through hanging drop approach. (a) (i) Actual image of the 384 hanging drop array plate highlighting the key features and specifications. (ii) Schematic of the hanging drop formation process in the array plate. Cell suspension is dispensed into the access hole to the bottom surface of the plate using pipette and within hours, individual cells start to aggregate and eventually form into a single spheroid after 1 day. (iii) Schematic showing the humidification chamber that was used to culture 3-D spheroids in the hanging drop array plate format. The 384 hanging drop array plate was sandwiched between a 96-well plate filled with distilled water. Reprinted by copyright permissions from [57,67]. (b) (i) Schematic of the embryonic body formation process using hanging drop with integrated bio-printing approach. This approach can be utilized to make 3-D cancer models. Droplets of cell-medium suspension were printed onto the lid of a Petri dish and were hung up for 24 h to allow for EB aggregation. The formed EBs were transferred to a 96-well plate for additional culture up to 96 h. (ii) Images of uniformed-sized EBs formed using bio-printing with various droplet sizes: 1, 4, 10, and 20 µl. (iii) Fluorescent images of EBs after 96 h of culture. Reprinted by copyright permissions from [68].

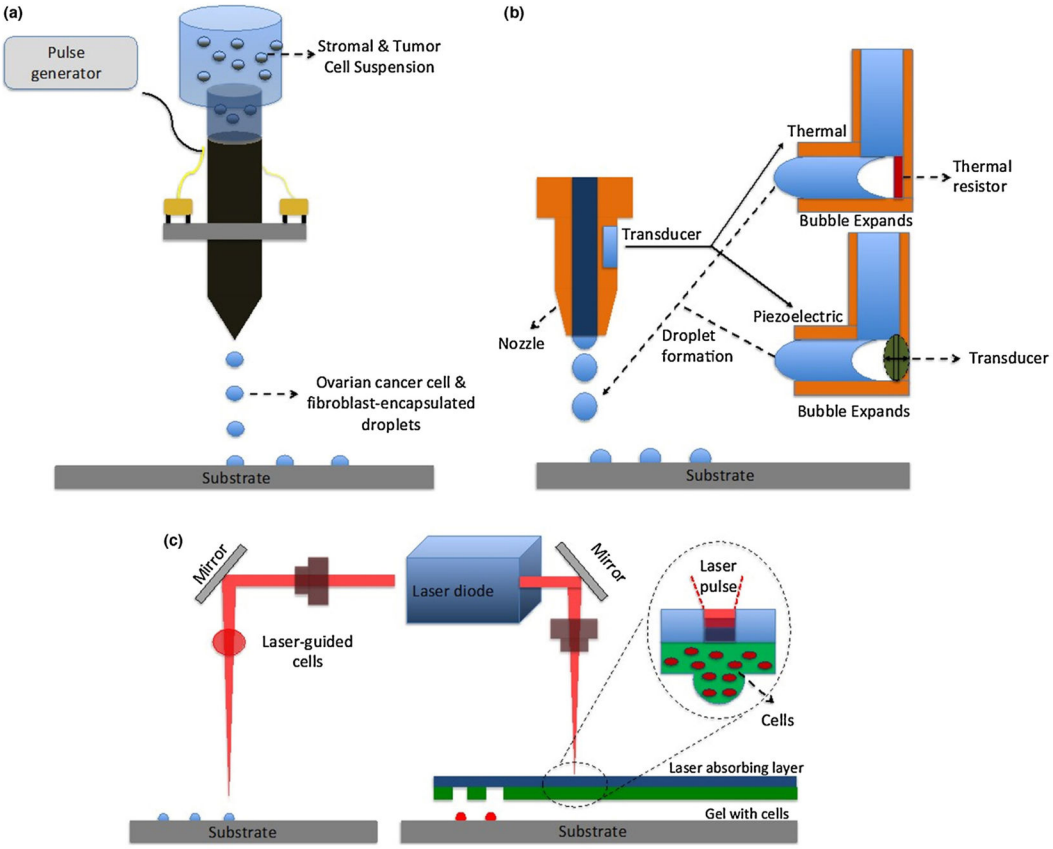

FIGURE 3.

Schematic of bio-printing technologies. (a) Schematic of the valve-based bio-printing setup used to make a 3-D co-culture of human ovarian cancer cells and fibroblasts. (b) Thermal and piezoelectric ink-jet printing. The thermal technique heats the resistor and expands the air bubbles. The piezoelectric technique charges crystals that expand. (c) Schematic of the laser printing setup where laser is focused into a cell suspension, and the optical force produced because of the difference in refractive indexes moves the cells onto an acceptor substrate. The cell-gel solution is propelled forward as a deposit by the pressure of a laser-induced vapor bubble (right).

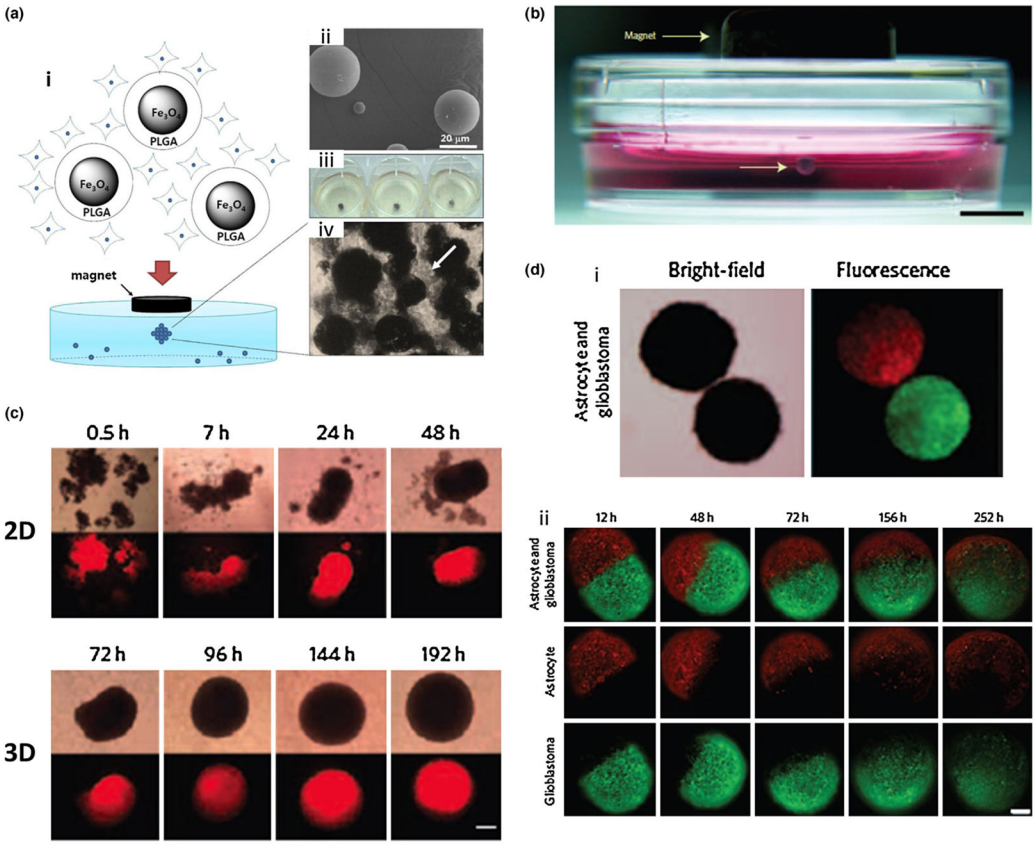

FIGURE 4.

Magnetic Fe_3O_4 encapsulated PLGA microparticles and iron oxide-containing hydrogels. (a) (i) Schematic representation of magnetic Fe_3O_4-loaded PLGA microparticles that were used for 3-D tumor spheroid cultures. (ii) SEM image of Fe_3O_4-loaded PLGA microparticles. (iii) Optical image of a cluster of KB tumor cells and PLGA microparticles. (iv) Optical image of KB tumor cell clusters (indicated by a white arrow) attached on the surface of magnetic PLGA microparticles. Reprinted by copyright permissions from [104]. (b) Human glioblastoma cells (lower arrow) mixed with magnetic Fe_3O_4-loaded containing hydrogel held at the air–medium interface by a magnet. Scale bar, 5 mm. (c) Comparison of 2-D with 3-D cell growth. Phase contrast (top row) and fluorescence (red, bottom row) images of levitated glioblastoma cells. The cells were monitored for 8 days. Scale bar, 200 mm. (d) Confrontation assay of magnetically levitated multicellular spheroids. (i) Bright-field and fluorescence images of human glioblastoma cells (green) and normal human astrocytes (red). The cells were cultured separately and then magnetically guided together. (ii) Images showing confrontation between human glioblastoma cells and normal astrocytes monitored for 10.5 days. Invasion of normal human astrocytes containing spheroid by human glioblastoma cells serves as a standard assay to analyze glioblastoma invasiveness. Scale bar, 200 mm. Reprinted by copyright permissions from [101].

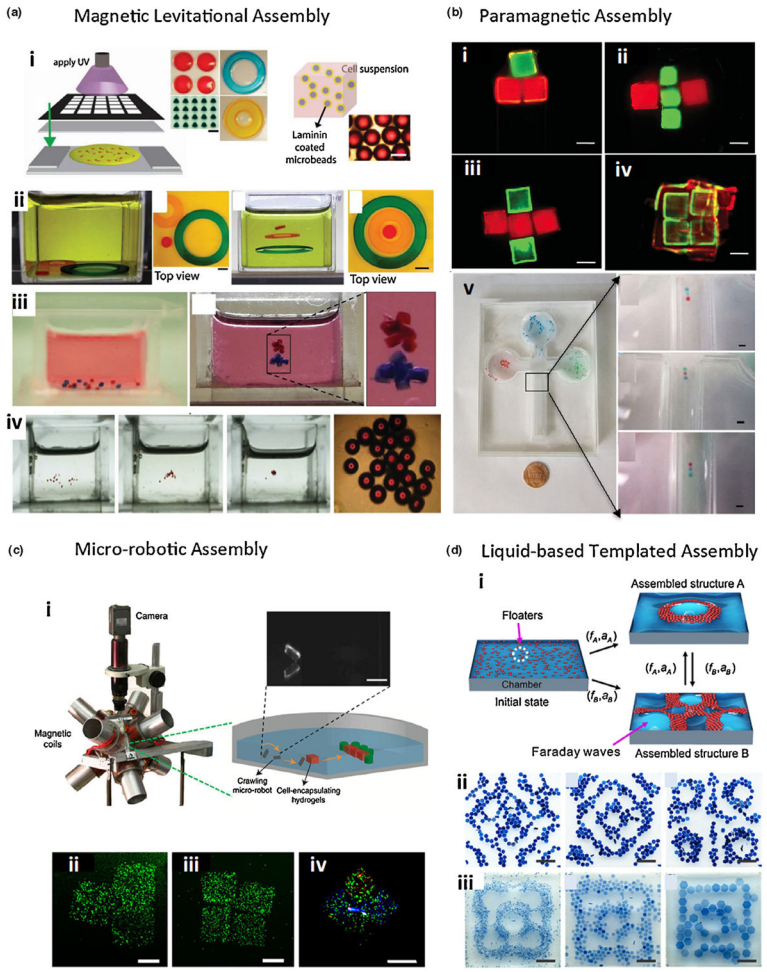

FIGURE 5.

(a) Fabrication and magnetic levitational soft living materials. Reprinted by copyright permissions from [108]. (i) Schematic of hydrogel and cell seeded microbead fabrication. (ii) Paramagnetic levitational self-assembly of soft components. (iii) Red and blue hydrogels assembled at different levels because of their polymer concentrations. (vi) 3T3 seeded microbeads were self-assembled with Paramagnetic levitation. The cross sections of the layers were obtained by cutting the assembled construct into two hemispheres. (b) Paramagnetic levitation assembly of MNP-free hydrogel. (i–iii) Various hydrogel assemblies. Hydrogels were labeled with FITC-dextran (green) and Rhodamine B. (red) indicating control over the assembled constructs. (iv) Merged fluorescent image of layer-by-layer 3-D assembly. Multi-layer 3-D constructs were fabricated by stacking layers of hydrogels. (v) Celtic-shaped patterning chamber. Each well is a reservoir for red, blue, or green hydrogels. Images show linear shape assembly of hydrogels with red gel at the front, in the middle, and at the back. Scale bar is 1 mm. Reprinted by copyright permissions from [95]. (c) Micro-robotic assembly of hydrogels and cells. (i) Magnetic coil system used to actuate magnetic micro-robots remotely. These untethered magnetic micro-robot were used to arrange hydrogels driven by magnetic field. Scale bar, 1 mm. Fluorescence images of National Institutes of Health (NIH) 3T3 mouse embryonic fibroblast cell-encapsulating

hydrogels after the assembly of (ii) T-shape and (iii) square-shape constructs. Scale bar, 500 μm. (iv) Fluorescence image of three-dimensional heterogeneous assembly of HUVEC, 3T3 and cardiomyocyte encapsulating hydrogels. Scale bar, 500 μm. Reprinted by copyright permissions from [96]. (d) Liquid-based templated assembly by Faraday waves. (i) Schematic demonstration of liquid-based templated assembly by Faraday waves. Dynamic reconfiguration of the assembled structures is achieved by setting vibrational parameters. (fA, a_A) and (f_B, a_B) are vibrational frequencies and accelerations for the formation of structures A and B, respectively. By tuning the initial chamber with (fA, a_A) and (f_B, a_B), assembly of the structures A and B from dispersed floaters can be performed, as well as the reversible transitions between the structures. (ii) Assembly of GelMA hydrogel units (dark blue) into various structures. (iii) Assembly of size-varied hydrogel units. PEG hydrogel units (light blue) with sizes of 0.5, 1, and 2 mm were assembled into the same pattern. Scale bars: 4 mm. Reprinted by copyright permissions from [110].

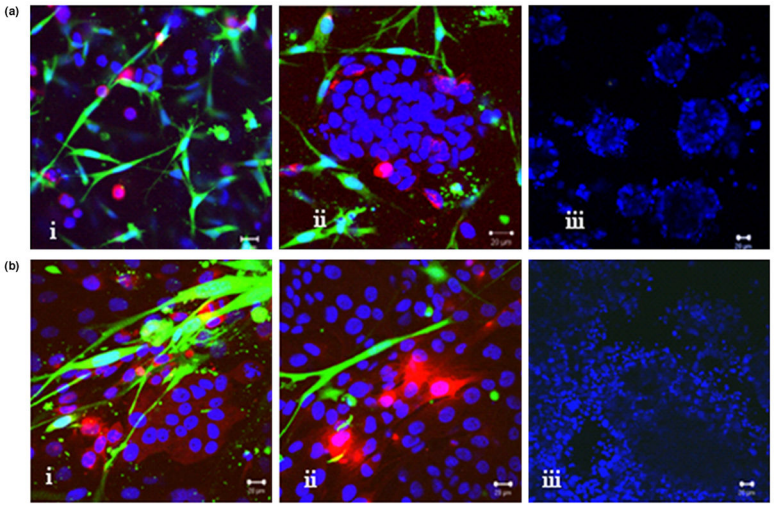

FIGURE 6.

Influence of fibroblast on co-units formations in collagen hydrogel. Fibroblast cells (green), myoepithelial cells (red) and MCF-7 cancer cells (blue). (a) (i) showed cell organization at the day 1. (ii) Cell organization at day 7 showed the homing of myoepithelial cells around the cluster of MCF-7 cancer cells. The normal fibroblast cells were arranged around the co-units and had no effect on co-unit formation. (iii) Low power image of co-units. (b) (i) and (ii) show the disruption of co-units once the tumor-associated fibroblast were added. (iii) Low power image of disrupted co-units. Reprinted by copyright permissions from [125]

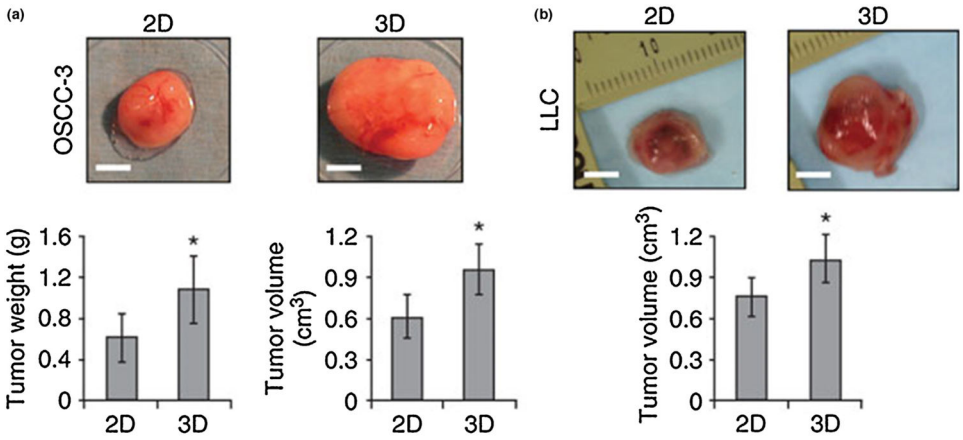

FIGURE 7.

Cancer cells were cultured on 3-D PLG scaffolds and 2-D culture plates before implanting in mouse models. (a) Tumor mass grown in mouse model after preculture of OSCC-3 cells in 3-D PLG scaffold (right) and 2-D culture plates (left). Tumor grown in 3-D model was of higher weight and volume. (b) Tumor mass grown in mouse model after preculture of mouse LLC cells in 3-D PLG scaffold (right) and 2-D culture plate (left). Scale bars are 5 mm in all images. Reprinted by permission from [37].

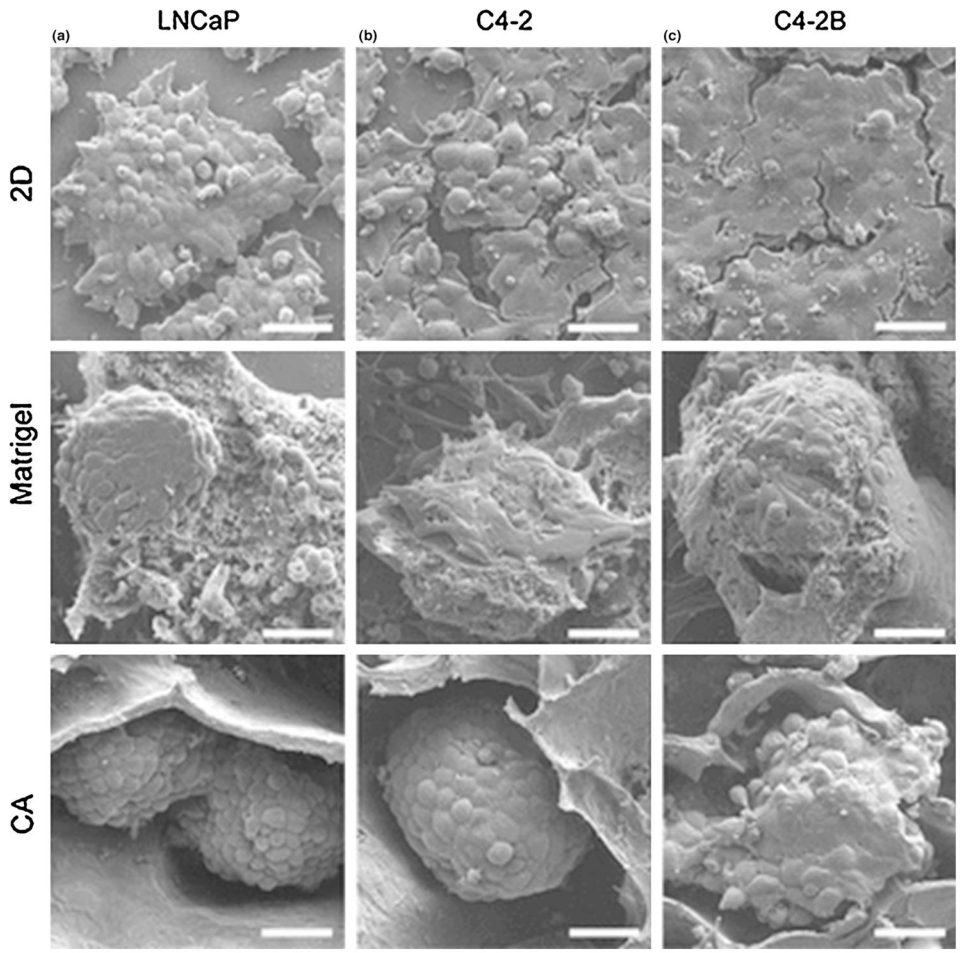

FIGURE 8.

Scanning electron microscope (SEM) images of the three cell lines of prostate cancer cells cultured in different models (2-D, Matrigel and Chitosan-Alginate (CA) 3-D model). (a) SEM images of LNCaP cancer cells. (b) SEM images of C4-2 cancer cells. (c) SEM images of C4-2B cancer cells. The 2-D culture formed flat cell sheets whereas Matrigel and CA 3-D cultures formed spheroids mimicking *in vivo* tumor growth. Scale bars are 40 μm. Reprinted by copyright permissions from [2].